Redox Biology 62 (2023) 102666

Contents lists available at ScienceDirect

Redox Biology

journal homepage: www.elsevier.com/locate/redox

Protective effects of an electrophilic metabolite of docosahexaenoic acid on UVB-induced oxidative cell death, dermatitis, and carcinogenesis

Seong Hoon Kim [a], So Eui Lee [b], Su-Jung Kim [a,b], Xizhu Fang [a], Jihyeon Hur [c], Erdi Sozen [d], Nesrin Kartal Özer [e], Kwang Pyo Kim [c,f,**], Young-Joon Surh [a,b,g,*]

[a] Research Institute of Pharmaceutical Sciences, College of Pharmacy, Seoul National University, Seoul, South Korea
[b] Department of Molecular Medicine and Biopharmaceutical Sciences, Graduate School of Convergence Science and Technology, Seoul National University, Seoul, South Korea
[c] Department of Applied Chemistry, Institute of Natural Science, Global Center for Pharmaceutical Ingredient Materials, Kyung Hee University, Yongin, South Korea
[d] Department of Biochemistry, Faculty of Medicine, Marmara University, Maltepe, Istanbul, Turkey
[e] Department of Biochemistry, Faculty of Medicine, Uskudar University, Altunizade, Istanbul, Turkey
[f] Department of Biomedical Science and Technology, Kyung Hee Medical Science Research Institute, Kyung Hee University, Seoul, South Korea
[g] Cancer Research Institute, Seoul National University, Seoul, South Korea

ARTICLE INFO

Keywords:
17-Oxo-DHA
Dermatitis
Photocarcinogenesis
Efferocytosis
Resolution of inflammation
UVB-induced inflammation

ABSTRACT

Docosahexaenoic acid (DHA), a representative omega-3 (ω-3) polyunsaturated fatty acids, undergoes metabolism to produce biologically active electrophilic species. 17-Oxo-DHA is one such reactive metabolite generated from DHA by cyclooxygenase-2 and dehydrogenase in activated macrophages. The present study was aimed to investigate the effects of 17-oxo-DHA on ultraviolet B (UVB)-induced oxidative stress, inflammation, and carcinogenesis in mouse skin. UVB-induced epidermal cell death was ameliorated by topically applied 17-oxo-DHA. Topical application of 17-oxo-DHA onto hairless mouse skin inhibited UVB-induced phosphorylation of the proinflammatory transcription factor, STAT3 on tyrosine 705 (Tyr705). The 17-oxo-DHA treatment also reduced the levels of oxidative stress markers, 4-hydroxynonenal-modified protein, malondialdehyde, and 8-oxo-2′-deoxyguanosine. The protective effects of 17-oxo-DHA against oxidative damage in UVB-irradiated mouse skin were associated with activation of Nrf2. 17-Oxo-DHA enhanced the engulfment of apoptotic JB6 cells by macrophages, which was related to the increased expression of the scavenger receptor CD36. The 17-oxo-DHA-mediated potentiation of efferocytic activity of macrophages was attenuated by the pharmacologic inhibition or knockout of Nrf2. The pretreatment with 17-oxo-DHA reduced the UVB-induced skin carcinogenesis and tumor angiogenesis. It was also confirmed that 17-oxo-DHA treatment significantly inhibited the phosphorylation of the Tyr705 residue of STAT3 and decreased the expression of its target proteins in cutaneous papilloma. In conclusion, 17-oxo-DHA protects against UVB-induced oxidative cell death, dermatitis, and carcinogenesis. These effects were associated with inhibition of STAT3-mediated proinflammatory signaling and also activation of Nrf2 with subsequent upregulation of antioxidant and anti-inflammatory gene expression.

1. Introduction

Skin interacts with the environment and is the first barrier against chemical toxicants, infectious pathogens, solar radiation, etc. The skin constantly adapts to external changes and maintains internal balance by regulating hormones, cytokines, and microbiota [1–3]. When such homeostasis is imbalanced due to excessive noxious stimuli and/or insufficient self-protection, this can cause skin rash, skin aging, immune system disorder, and cancer [4,5].

Continuous exposure to solar light, especially ultraviolet B (UVB), results in physical and biological changes in the skin barrier which can induce dermatitis and photocarcinogenesis [6,7]. In this process, the UVB-damaged epithelial cells transmit the signals to tissue-resident cells. As a result, phagocytes including macrophages and neutrophils

* Corresponding author. Research Institute of Pharmaceutical Sciences, College of Pharmacy, Seoul National University, Seoul, South Korea.
** Corresponding author. Department of Applied Chemistry, Institute of Natural Science, Global Center for Pharmaceutical Ingredient Materials, Kyung Hee University, Yongin, South Korea.
E-mail addresses: kimkp@khu.ac.kr (K.P. Kim), surh@snu.ac.kr (Y.-J. Surh).

https://doi.org/10.1016/j.redox.2023.102666
Received 31 January 2023; Received in revised form 4 March 2023; Accepted 8 March 2023
Available online 9 March 2023

directly recognize and destroy the pathogens, while dendritic cells mediate adaptive immune response by modulating T cell differentiation [8]. Neutrophils have long been considered short-lived frontline cells of innate immunity, with a primary function against acute inflammation. Since neutrophils have a short lifespan, the subsequent reactions are mainly regulated by macrophages [9].

Acute inflammation is a self-limiting process for tissue repairing and the restoration of homeostasis [10]. If acute inflammation is not adequately resolved, the inflammatory response can persist and trigger the pathogenesis of several chronic disorders such as asthma, arthritis, atherosclerosis, and even cancer [11]. Apoptosis is the most prominent process of programmed cell death observed in the resolution phase of tissue. Since the accumulation of dead or dying cells triggers or exacerbates a persistent inflammatory response, the elimination of apoptotic cells is essential for the proper termination of acute inflammation [12].

Efferocytosis is a process by which dead/dying cells are removed by the phagocytic activity of macrophages [13,14]. Various scavenger receptors, including CD36, present on the surface of macrophages recognize those cells that are supposed to be phagocytosed. Efferocytosis is hence critical in preventing secondary necrosis and intensification of inflammation, contributing to the resolution of inflammation.

Signal transducer and activator of transcription 3 (STAT3), a representative proinflammatory transcription factor, promotes cell growth by upregulating target proteins including c-Myc and Cyclin D1 [15]. Activated STAT3 augments inflammatory signaling and disrupts the balance of homeostasis, thereby contributing to chronic inflammation and carcinogenesis [16].

Nrf2 is an essential transcription factor that plays a pivotal role in chemoresistance and biological defense by upregulating the expression of many antioxidative and anti-inflammatory enzymes, such as heme oxygenase-1 (HO-1) and NAD(P)H:quinone oxidoreductase 1 (NQO1), and other cytoprotective proteins [17]. In this context, Nrf2 is the master regulator of cellular adaptive stress response to maintain/restore the homeostasis [18].

The acute inflammatory response can be divided into initiation and resolution phases. A group of specialized pro-resolving mediators (SPMs) have emerged as endogenous substances involved in the resolution of acute inflammation. SPMs are enzymatically synthesized from ω-3 polyunsaturated fatty acids, including docosahexaenoic acid (DHA) [19,20]. They are capable of limiting polymorphonuclear neutrophil infiltration and enhancing macrophage clearance of apoptotic cells [21]. In a previous study, we demonstrated that topically applied DHA alleviated UVB-induced inflammation and carcinogenesis in mouse skin [22].

DHA undergoes alternative metabolism to produce a series of biologically reactive electrophilic fatty acids [23]. 17-Oxo-DHA is one such electrophilic metabolite generated by cyclooxygenase-2 (COX-2) and dehydrogenase activities of macrophages recruited in the inflamed sites. Though 17-oxo-DHA was reported to inhibit the inflammatory signaling [24–26], its anti-inflammatory and chemoprotective/chemopreventive effects *in vivo* have not been reported yet. In the present study, we explored the effects of 17-oxo-DHA on UVB-induced oxidative cell death, dermatitis and carcinogenesis in mouse skin.

2. Materials and Methods

2.1. Chemicals and reagents

17-Oxo-DHA (4Z,7Z,10Z,13Z,15E,19Z-17-oxo-docosahexaenoic acid) was purchased from Cayman Chemical Co. (Ann Arbor, MI, USA). Dulbecco's modified Eagle's medium (DMEM), Minimum Essential Media (MEM), fetal bovine serum (FBS), sodium pyruvate, and gentamicin were supplied by Gibco (Grand Island, NY, USA). Trypsin and ethylenediaminetetraacetic acid (EDTA) were purchased from Welgene (Gyeongsan-si, Gyeongsangbuk-do, South Korea). The primary antibodies for detecting 4-hydroxynonenal (4-HNE) and malondialdehyde (MDA) were provided by the Japan Institute for the Control of Aging (JaICA), Nikken SEIL Co., Ltd. (Shizuoka, Japan). Anti-8-hydroxy-2′-deoxyguanosine (8-oxo-dG) antibody was purchased from TREVIGEN® (Gaithersburg, MD, USA). Antibodies for STAT3, P-STAT3^{Y705}, and c-Myc were supplied by Cell Signaling Technology (Danvers, MA, USA). The antibodies for NQO1, β-actin, and CD36 were obtained from Santa Cruz Biotechnology (Dallas, TX, USA). Anti-Nrf2 and Anti–HO–1 were the products of Abcam (Cambridge, MA, USA) and Enzo Life Sciences (Farmingdale, NY, USA), respectively. pHrodo Red and 4′,6-diamidino-2-phenylindole (DAPI) were obtained from Thermo Fisher Scientific (Waltham, MA, USA). Theantibodies against F4/80, recombinant mouse M-CSF, and red blood cell lysis buffer were supplied by Biolegend (San Diego, CA, USA). ML385 (N-[4-[2,3-Dihydro-1-(2-methylbenzoyl)-1H-indol-5-yl]-5-methyl-2-thiazolyl]-1,3-benzodioxole-5-acetamide) was the product of Sigma-Aldrich Co. (St. Louis, MO, USA).

2.2. UVB-induced dermatitis

Female SKH1-*Hr*^{hr} mice (5–6 weeks of age) were obtained from Orient Bio Inc. (Seongnam-si, Gyeonggi-do, South Korea). Mice were randomly divided into four groups ($n = 3$ per group) and housed in plastic cages under the controlled conditions of temperature (23 ± 2 °C), humidity (50 ± 10%), and light (12/12 h light/dark cycle). All experiments on animals complied with the Guide for the Institutional Animal Care and Use Committee (IACUC) at Seoul National University (Approval number; SNU-190812-2). For the UVB irradiation, 5 × 8 Watts tubes were used, which emit wavelengths mainly in the 312 nm UVB region. Mice were irradiated with UVB (180 mJ/cm^2 and 500 mJ/cm^2) using the Biolink BLX-312 UV crosslinker (Vilber Lourmat; Marne-la-Vallée, Paris, France). 17-Oxo-DHA (20 nmol) was dissolved in 200 μL of acetone and topically treated onto the dorsal skin of mice. The degree of UVB-induced inflammation was identified by the clinical skin score system based on the symptoms consisting of erythema, scarring, edema, and erosion. Each of these symptoms was rated on a scale of 0–3. The thickness of the dorsal skin was measured by a caliper.

2.3. UVB-induced skin carcinogenesis

Female SKH1-*Hr*^{hr} mice (5–6 weeks of age) were randomly divided into three groups ($n = 7$ per group). The mice were irradiated with UVB (180 mJ/cm^2) using the Biolink BLX-312 UV crosslinker (Vilber Lourmat; Marne-la-Vallée, Paris, France) three times a week for 26 weeks. 17-Oxo-DHA (20 nmol) dissolved in 200 μL of acetone was topically applied onto the dorsal skin of mice 30 min prior to each UVB exposure. Mice were euthanized and their skin tissues were collected for adequate analysis.

2.4. Histological analysis

The parts of skin biopsies were fixed with 10% phosphate-buffered formalin and embedded in paraffin. The skin sections were stained with hematoxylin and eosin (H&E). The H&E stained tissue sections were visualized under a light microscope (Nikon; Tokyo, Japan) to verify the presence of inflammatory lesions.

2.5. Immunohistochemical analysis

The dissected mouse skin tissues were prepared for immunohistochemical analysis with primary antibodies against 4-HNE, MDA (JaICA; Shizuoka, Japan), and 8-oxo-dG (TREVIGEN®; Gaithersburg, MD, USA). Four-micrometer sections of 10% formalin-fixed, paraffin-embedded tissues were deparaffinized and rehydrated in a series of xylene and ethanol buffer. The sections were heated in a microwave and boiled twice for 6 min in a 10 mM citrate buffer (pH 6.0) for antigen retrieval. To reduce nonspecific staining, each section was treated with 3% hydrogen peroxide and 4% peptone casein blocking solution for 15 min.

The slides were incubated with a diluted primary antibody at room temperature for 40 min in Tris-HCl-buffered saline containing 0.05% Tween 20, followed by incubation with a horseradish peroxidase-conjugated secondary antibody (Dako; Glostrup, Denmark). The tissues were treated with 3,3′-diaminobenzidine (DAB) tetrahydrochloride to detect the peroxidase binding sites. Finally, counterstaining was performed with Mayer's hematoxylin. Quantification of immunohistochemical images was carried out by using the ImageJ/Fiji software. Positively DAB-stained tissue were quantified at 5 randomly selected fields for each sample.

2.6. Immunofluorescence staining

The mouse skin specimens were fixed, paraffin-embedded, and sectioned, and the sections were deparaffinized and rehydrated by serial washes with graded xylene and alcohol. For immunofluorescence staining, tissue sections were boiled in 10 mM of sodium citrate (pH, 6.0) for antigen retrieval, subjected to serial washing with phosphate-buffered saline (PBS), and permeabilized for 45 min at room temperature using 0.2% Triton X-100 in PBS and blocked with 3% bovine serum albumin (BSA) in PBS for 1 h at room temperature. The skin tissue sections were stained with primary antibodies for P-STAT3, Nrf2 (Cell Signaling Technology; Danvers, MA, USA), and F4/80 (Biolegend; San Diego, CA, USA) diluted at 1:250 in 3% BSA overnight at 4 °C. After washing three times with PBS each 5 min, tissues were incubated with appropriate secondary antibodies. Nuclei were counterstained with DAPI (Invitrogen; Carlsbad, CA, USA). Immunofluorescence images were visualized under a fluorescence microscope (Nikon; Tokyo, Japan).

2.7. Terminal Deoxynucleotidyl Transferase dUTP Nick end labeling (TUNEL) assay

The apoptotic DNA fragmentation was measured by the TUNEL assay with the ApopTag® Peroxidase *In Situ* Apoptosis Detection Kit (Chemicon; Temecula, CA, USA). The isolated mouse skin tissues were rinsed with PBS and fixed in 10% buffered formalin (Sigma-Aldrich; Saint Louis, MO, USA) for the TUNEL assay. The apoptotic cells were detected under a light microscope (Nikon; Tokyo, Japan).

2.8. Lysis of tissue and protein extraction

The UVB-treated mouse dorsal skin was collected, and fat was removed on ice to attain the epidermal layer. Collected epidermis was homogenized with the lysis buffer (20 mM Tris-HCl (pH 7.5), 150 mM NaCl, 1 mM Na_2EDTA, 1 mM EGTA, 1% Triton, 2.5 mM sodium pyrophosphate, 1 mM β-glycerophosphate, 1 mM Na_3VO_4, 1 μg/mL leupeptin, 1 mM phenylmethyl sulfonylfluoride (PMSF), and an EDTA-free cocktail tablet) in an ice bath. The whole lysates were vortexed every 10 min for 3 h on the ice, followed by centrifugation (13,000×*g*, 15 min at 4 °C). The supernatants were collected and stored at −70 °C until use.

2.9. Cytosolic and nuclear extraction

The fat-free dorsal skin tissues were homogenized with 1 mL buffer A [10 mM 4-(2-hydroxyethyl)-1-piperazineethanesulfonic acid (HEPES, pH 7.8), 1.5 mM $MgCl_2$, 10 mM KCl, 0.5 mM dithiothreitol (DTT), and 0.2 mM PMSF] followed by vortex-mixing every 10 min for 3 h in an ice bath. The lysates were mixed with 0.1% Nonidet P-40 (NP-40) 30 min before centrifugation. After centrifugation at 13,000×*g* for 15 min, the supernatants (the cytosolic extracts) were obtained. The precipitated nuclear pellets were washed three times with buffer A containing 0.625% NP-40 to remove a residual cytosolic fraction. Nuclear pellets were then resuspended in 300 μL of buffer C [20 mM HEPES (pH 7.8), 420 mM NaCl, 1.5 mM $MgCl_2$, 0.2 mM EDTA, 0.5 mM DTT, 0.2 mM PMSF, and 20% glycerol]. The nuclear lysates were vortexed every 10 min for 1 h, followed by centrifugation at 13,000×*g* for 15 min. The supernatants (nuclear extracts) were collected and kept at −70 °C until use.

2.10. Western blot analysis

The protein concentration of lysates was measured by the Pierce™ BCA Protein Assay Kit (Thermo Fisher Scientific; Rockford, IL, USA). The lysates were loaded on 8–15% SDS-polyacrylamide gel for performing electrophoresis under reducing conditions. Protein was transferred to the polyvinylidene difluoride membrane (PALL Life Sciences; Washington, NY, USA). The membranes were blocked with 5% non-fat dry milk in Tris-buffered saline containing 0.1% Tween 20 (TBST) for 1 h at room temperature. Each blot was incubated with its respective primary antibody diluted in TBST at 4 °C overnight. The membranes were rinsed three times for 10 min with TBST buffer. Then, washed blots were probed with 1:5000 dilution of horseradish peroxidase-conjugated secondary antibody (Invitrogen; Carlsbad, CA, USA) for 1 h at room temperature and washed three times again with TBST buffer. The immunoblots with protein-antibody complexes were visualized with an enhanced chemiluminescent (ECL) detection kit (Abclon; Seoul, South Korea) and LAS-4000 image reader (Fujifilm; Tokyo, Japan).

2.11. Quantitative real-time polymerase chain reaction (qPCR)

Total RNA was isolated from mouse skin tissues with Trizol® (Invitrohen; Carlsbad, CA, USA), and the reverse transcription reaction was conducted using the Moloney murine leukemia virus (M-MLV) reverse transcriptase (Promega; Madison, WI, USA) to synthesize the complementary DNA (cDNA). qPCR was carried out with a 7500 Real-Time PCR instrument (Applied Biosystems; Foster City, CA, USA) using the RealHelix™ qPCR Kit (Green) (NanoHelix Co. Ltd.; Daejeon, South Korea). The primers used for each qPCR reactions are as follows; *Il6*, 5′-TCT ATA CCA CTT CAC AAG TCG GA-3' and 5′-GAA TTG CCA TTG CAC AAC TCT TT-3'; *Tnf*, 5′-CAG GCG GTG CCT ATG TCT C-3' and 5′-CGA TCA CCC CGA AGT TCA GTA G-3'; *Actb*, 5′-GGC TGT ATT CCC CTC CAT CG-3' and 5′-CCA GTT GGT AAC AAT GCC ATG T-3' (forward and reverse, respectively). Target gene expression was normalized to actin. The relative gene expression was analyzed by the comparative cycle threshold (Ct) (ΔΔCt) method.

2.12. Cytokines analysis

The lysate of mouse skin tissues was analyzed using ELISA kits according to the manufacturer's instruction. Mouse IL-6 and TNF-α ELISA kits were obtained from RayBiotech (Norcross, GA, USA).

2.13. Isolation of bone marrow-derived macrophages (BMDMs)

The femur and tibia were harvested from mice. After cutting both ends of the bone, bone marrow was flushed out by cold PBS. The cells from bone marrow were filtered through a 100 μm FALCON nylon cell strainer (Thermo Fisher Scientific; Waltham, MA, USA) and centrifuged at 500×*g* for 5 min at 4 °C. The cell pellet was resuspended and incubated with red blood cell lysis buffer for 1 min at room temperature. After discarding the lysis buffer, the isolated cells were plated in DMEM containing 20 ng/mL M-CSF and incubated at 37 °C in a humidified incubator containing 5% CO_2 for 4 days. Cells were then switched to media supplemented with 10 ng/mL M-CSF for 3 days.

2.14. Efferocytosis assay

The mouse epidermal JB6 Cl4 cells (American Type Culture Collection; Manassas, VA, USA) were incubated with 5% MEM media. JB6 Cl4 cells were irradiated with UVB (200 mJ/cm^2) and incubated at 37 °C and 5% CO_2 for 24 h. Apoptotic cells induced by UVB radiation were collected and stained with pHrodo Red for 30 min at 37 °C. The dead

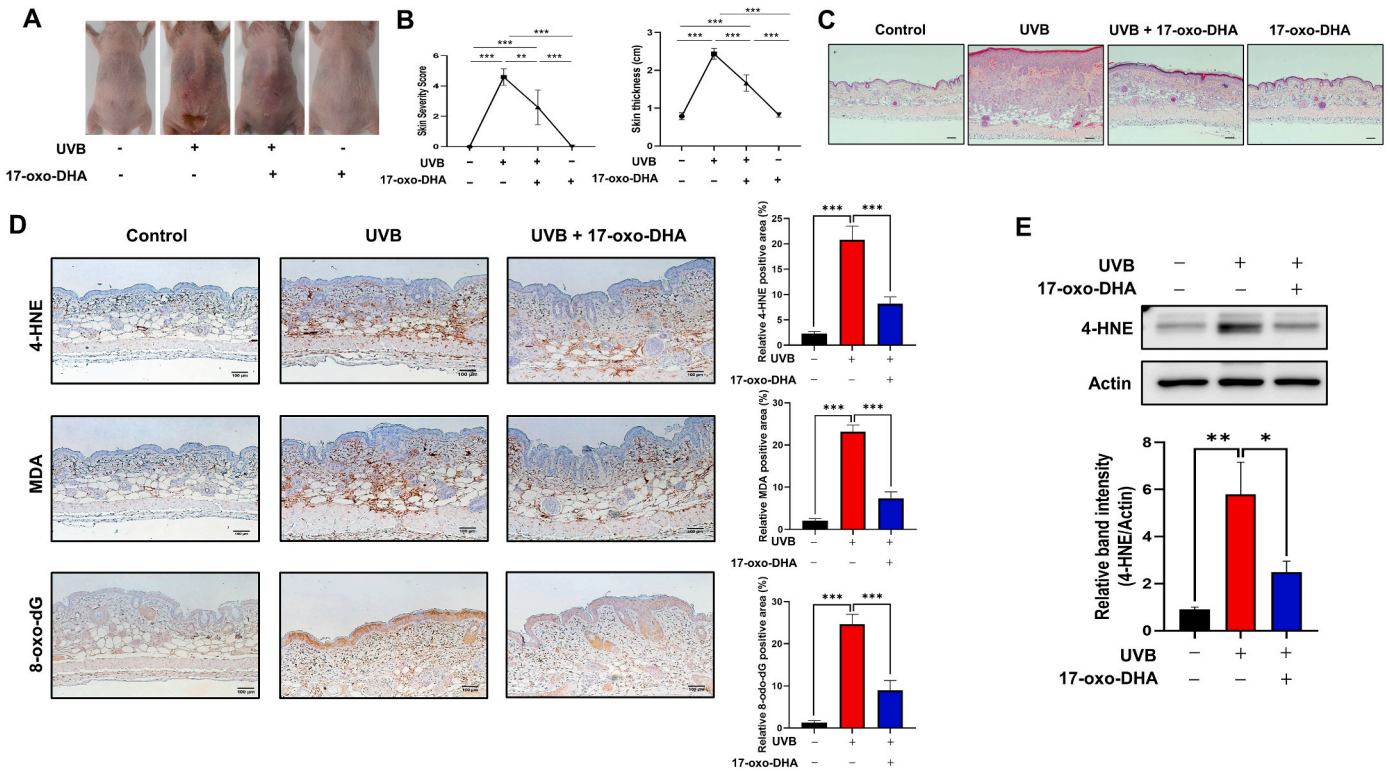

Fig. 1. Protective effects of topically applied 17-oxo-DHA on UVB-induced inflammation and oxidative stress in mouse skin.
17-Oxo-DHA (20 nmol) was topically applied for four days onto the dorsal skin of hairless female SKH1-*Hr*^{hr} mice after single UVB irradiation (500 mJ/cm^2). Twenty-four hours later, skin tissues were collected for histological and biochemical analyses. (A) The photographic images represent the wound of each group after the UVB irradiation. (B) Skin severity was scored based on the symptoms, and skin thickness was measured with a caliper. (C) Paraffin-embedded skin tissue blocks were stained with H&E. Magnification, 100 ×; Scale bar, 200 μm. Female hairless mice were topically applied with 17-oxo-DHA (20 nmol) 30 min before UVB irradiation (180 mJ/cm^2). (D) The paraffin sections of epidermal tissue were immunostained for 4-HNE, MDA, and 8-oxo-dG. Magnification, 200 X; Scale bar, 100 μm. (E) The protein levels of 4-HNE in UVB-induced mouse skin with or without 17-oxo-DHA treatment were measured by Western blot analysis. Data are expressed as means ± SD (n = 3 per group). *$p < 0.05$; **$p < 0.01$; ***$p < 0.001$.

epithelial cells were centrifuged at 300×*g* for 3 min and washed twice with PBS. To the 1 × 10^6 BMDMs in a 60 mm plate, 3 × 10^6 pHrodo-labelled apoptotic cells were added followed by co-incubation at 37 °C for 1 h. After the incubation, these plates were washed twice with PBS to remove residual apoptotic cells.

2.15. Estimation of hemoglobin

The tissue lysate was used to measure the amount of hemoglobin with Drabkin's reagent (Sigma-Aldrich; St. Louis, MO, USA). After the mixed well with the reagent, absorbance at 540 nm was detected to estimate the content of hemoglobin in mouse skin tissue.

2.16. Flow cytometry assay

Adherent cells were detached from the plates by treating 5 mM EDTA and spun down at 500 *g* for 5 min at 4 °C. Following the removal of unwanted debris-free isotype control antibody, incubation with CD16/32 antibody was performed to block the non-specific binding of other antibodies. After blocking, F4/80 antibody was added and incubated for 30 min at 4 °C. Prepared samples were detected by FACS Calibur™ flow cytometer (Becton, Dickinson and Company; Franklin Lakes, NJ, USA) and analyzed with FlowJo software.

2.17. Sample preparation for LC-MS/MS analysis

Recombinant STAT3 protein (Abcam; Cambridge, MA, USA) treated with 17-oxo-DHA was digested by the in-solution method. To this, 6 M urea in 50 mM ammonium bicarbonate (pH 8.0) was added to denature the proteins. The proteins were incubated for 1 h at 37 °C with 10 mM DTT and then alkylated with 30 mM iodoacetic acid (IAA). The MS-grade trypsin protease was added and incubated at 37 °C overnight (enzyme-to-protein ratio = 1: 10). The peptides were desalted using Pierce® C-18 spin columns and dried using Speed-Vac.

2.18. Direct infusion mass spectrometry (DIMS) analysis of 17-oxo-DHA

17-Oxo-DHA was reconstituted in 50% methanol and loaded in a Hamilton syringe. The sample was injected by a syringe pump with a flow rate of 5 μL/min into the heated electrospray ionization (HESI) source and measured for 30 s on a Q-Exactive HF-X Hybrid Quadrupole orbitrap mass spectrometer (Thermo Fisher Scientific; San Jose, CA, USA). The source conditions for MS scan in the negative electrospray ionization (ESI) mode were optimized: spray voltage, 3.8 kV; heated capillary temperature, 320 °C; nitrogen was used as damping gas. MS scans were acquired for the mass range of 340.2–342.2 *m/z* at a resolution of 60,000 in MS1 level and 15,000 for high-energy collision dissociation (HCD) experiments and normalized collision energies (NCE) was set at 27.

2.19. LC-MS/MS analysis

For LC-MS/MS analysis, Ultimate 3000 UHPLC system (Thermo Fisher Scientific; San Jose, CA, USA) was coupled to Q-Exactive HF-X Hybrid Quadrupole orbitrap mass spectrometer (Thermo Fisher Scientific) equipped with analytical columns (EASY-Spray™ LC Columns, C18, 75 μm × 50 cm, 2 μm, 100 Å; Thermo Fisher Scientific) and trap columns (C18, 75 μm × 2 cm, 3 μm, 100 Å, Thermo Fisher Scientific).

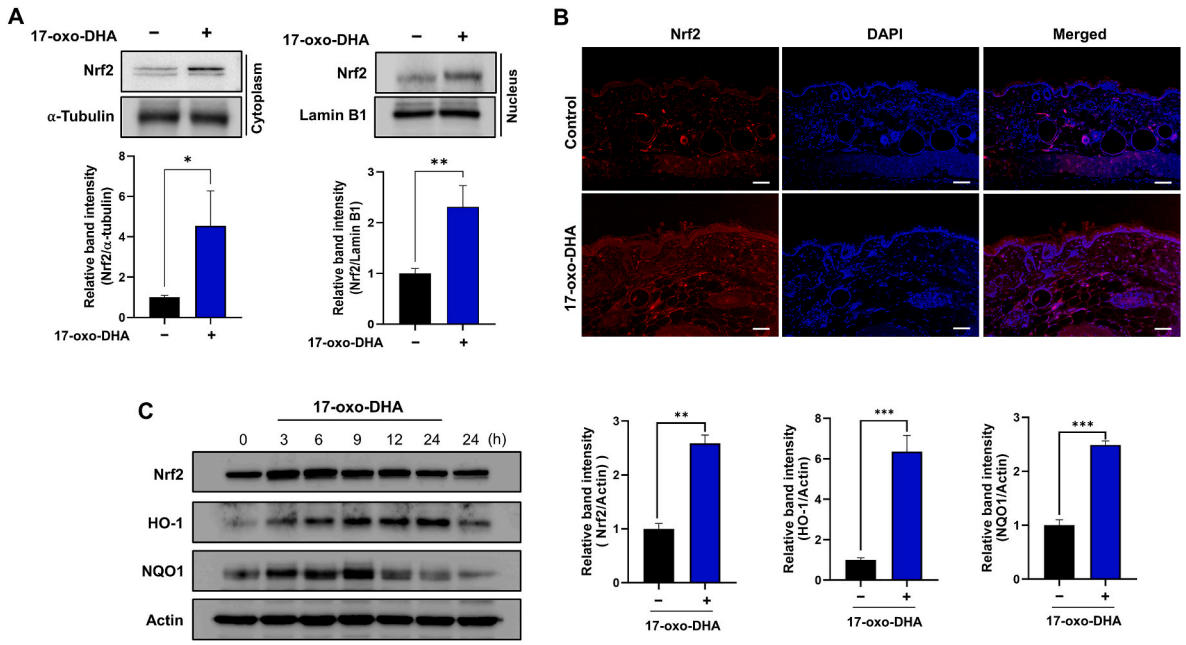

Fig. 2. Enhanced nuclear translocation of Nrf2 and its target protein expression in 17-oxo-DHA treated mice. (A, B) The accumulation of Nrf2 in cytoplasm and nucleus was verified by immunoblot analysis (A) and immunofluorescence staining (B). Magnification, 100 X; Scale bar, 200 μm. (C) Dorsal skins of mice were applied with 20 nmol 17-oxo-DHA for the indicated time. The histograms represent the data at 6 h. Protein lysates were isolated and subjected to Western blot analysis to measure the expression levels of Nrf2 and target proteins. Data are expressed as means ± SD (n = 3 per group). $^{*}p < 0.05$; $^{**}p < 0.01$; $^{***}p < 0.001$.

The peptide samples were separated by the mobile phase comprising of 0.1% formic acid in water (solvent A) and 0.1% formic acid in 90% acetonitrile (solvent B). The gradient condition was set as follows: (T min/% of solvent B) 0/2, 6/2, 10/10, 65/40, 90/60, 99/90, 104/90, 105/2, 120/2. The column temperature was set at 60 °C and the flow rate of the mobile phase was 300 nL/min.

The source conditions for MS scan in the positive ESI mode were optimized: spray voltage, 1.5 kV; heated capillary temperature, 250 °C; nitrogen was used as damping gas. The MS1 scan range was set of 350-2,000 *m/z* and the resolution was set at 60,000. The 12 most abundant

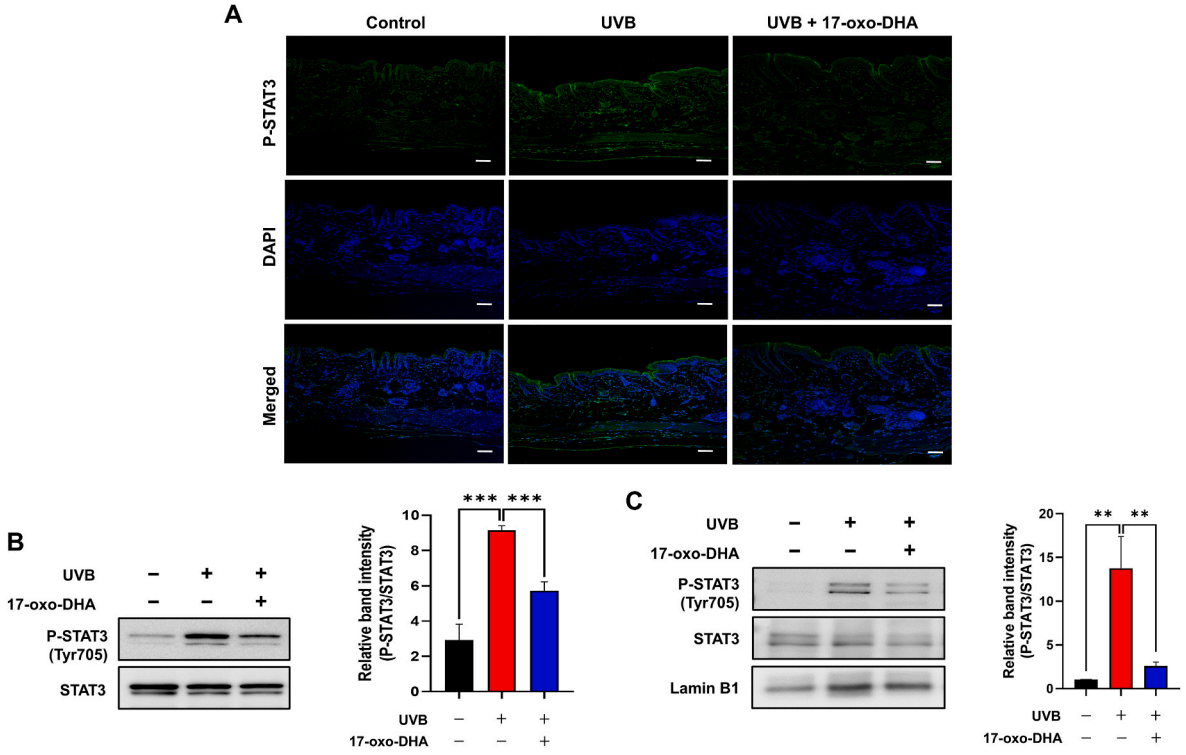

Fig. 3. Attenuation of UVB-induced STAT3 phosphorylation in mouse skin treated with 17-oxo-DHA. (A) The expression of P-STAT3 was measured by immunofluorescence staining. Magnification, 100 X; Scale bar, 200 μm. (B, C) Total protein lysate (B) and nuclear extract (C) were used for Western blot analysis to determine the levels of P-STAT3. Data are expressed as means ± SD (n = 3 per group). $^{**}p < 0.01$; $^{***}p < 0.001$.

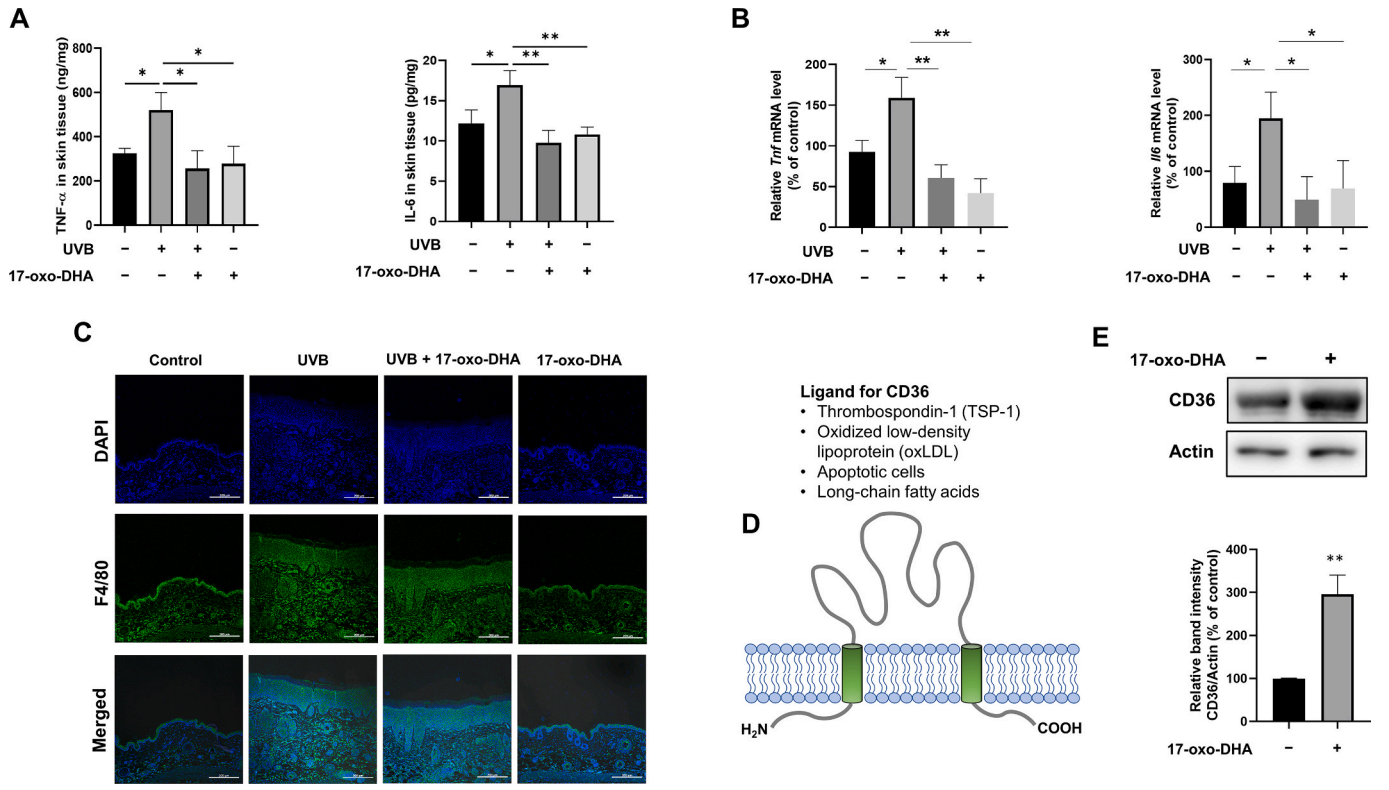

Fig. 4. 17-Oxo-DHA-mediated acceleration of the resolution of UVB-induced inflammation in mouse skin. (A) The amounts of TNF-α and IL-6 in mouse skin were determined by ELISA. (B) Tissue lysates were subjected to Real-Time Quantitative PCR to determine the mRNA levels of the same targets. (C) The macrophages were identified with F4/80 as a definitive marker and visualized by immunofluorescence staining. Magnification, 200 ×; Scale bar, 200 μm (D) The biological functions of CD36, a representative scavenger receptor present in macrophages. (E) The expression level of CD36 was measured by immunoblot analysis. Data are expressed as means ± SD (n = 3 per group). *$p < 0.05$; **$p < 0.01$.

ions were selected from MS1 scan and fragmented by data-dependent mode at a resolution of 15,000. MS2 scans were acquired with the dynamic exclusion for 30 s, an isolation window of 1.2 *m/z* and NCE of 27.

2.20. Statistical analysis

All the data were analyzed by mean ± standard deviation (SD) of at least three independent experiments. The Student's *t*-test determined statistical significance. All the statistical analyses were applied using GraphPad Prism 8.0 (GraphPad Software; San Diego, CA, USA). The value of $p < 0.05$ was considered statistically significant.

3. Results

3.1. UVB-induced dermatitis and oxidative stress were attenuated in 17-oxo-DHA treated mice

In order to assess the anti-inflammatory effects of 17-oxo-DHA, the UVB-induced mouse dermatitis model was employed (Supplementary Fig. 1). Four days after UVB irradiation, when the severity of the inflammation peaked, 17-oxo-DHA (20 nmol) was topically applied to the dorsal skin. On the fifth day of the experiment, mice were euthanized, and the lysates of skin tissue were prepared for subsequent analyses. The clinical skin score evaluated the degree of UVB-induced dermatitis based on symptoms of erythema, edema, scarring, and erosion. The topical application of 17-oxo-DHA accelerated resolution of inflammation (Fig. 1A). Mice treated with 17-oxo-DHA had a lower skin severity score and the reduced thickness of dorsal skin measured by a digital caliper (Fig. 1B), which was verified by H&E staining (Fig. 1C). The UVB irradiation can cause apoptosis (Supplementary Fig. 2), lipid peroxidation, and DNA fragmentation. 4-HNE and MDA are ubiquitously used as markers of oxidative tissue damage, and the formation of 8-oxo-dG is an indication of DNA damage. Topically applied 17-oxo-DHA attenuated the accumulation of 4-HNE, MDA, and 8-oxo-dG in mouse skin (Fig. 1D and E).

3.2. 17-Oxo-DHA enhanced the expression of cytoprotective proteins through Nrf2 activation in mouse skin

The redox-sensitive transcription factor Nrf2 is involved in cellular protection against oxidative and inflammatory stresses. To investigate whether the 17-oxo-DHA-induced potentiation of cytoprotective capacity contributes to the reduction of oxidative and inflammatory damage caused by UVB irradiation, we first measured the level of Nrf2 in the skin of 17-oxo-DHA-treated mice. The expression level of Nrf2 was elevated in both cytoplasm and nucleus of 17-oxo-DHA treated mouse skin as measured by immunoblot (Fig. 2A) and immunofluorescence (Fig. 2B) analyses. The expression of Nrf2 was transiently upregulated upon treatment with 20 nmol 17-oxo-DHA, which was accompanied by upregulation of its major target proteins, HO-1 and NQO1 in a time-dependent manner (Fig. 2C).

3.3. UVB-induced phosphorylation of STAT3 was reduced by topical application of 17-oxo-DHA

Aberrant overactivation of STAT3 is implicated in dermatitis and photocarcinogenesis [27]. STAT3 is activated through phosphorylation of its Tyr705 residue which facilitates the dimerization. The dimerized STAT3 translocates to the nucleus and binds to the promotor regions of target genes. The topical application of 17-oxo-DHA diminished the Tyr705 phosphorylation of STAT3 in mouse epidermis, as confirmed by the immunofluorescence staining (Fig. 3A) and Western blot analysis

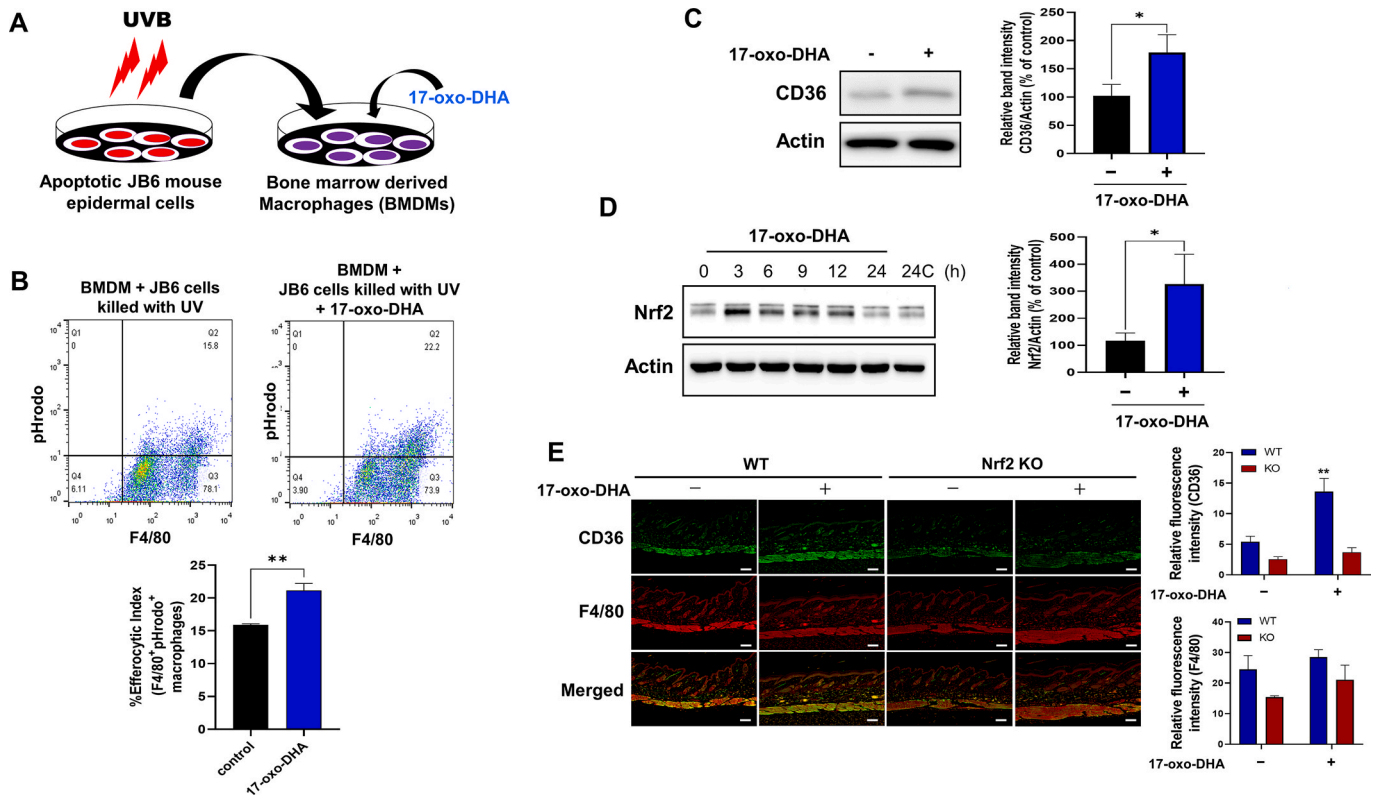

Fig. 5. Nrf2-mediated enhancement of efferocytosis activity of macrophages by 17-oxo-DHA. (A) BMDMs were treated with 17-oxo-DHA (5 μM) for 12 h, and co-incubated with apoptotic JB6 mouse epidermal cell debris for 1 h. (B) The flow cytometric analysis to assess the efferocytosis capability of macrophages. BMDMs were treated with 17-oxo-DHA (5 μM) for 24 h. The expression of CD36 (C) and Nrf2 (D) was measured by immunoblot analysis. (E) Fixed skin tissues were stained with anti-CD36 (green) or anti-F4/80 (red) antibody, and counterstained with DAPI (blue). Magnification, 200 ×; Scale bar, 100 μm. Data are expressed as means ± SD (n = 3 per group). *$p < 0.05$; **$p < 0.01$. (For interpretation of the references to colour in this figure legend, the reader is referred to the Web version of this article.)

(Fig. 3B). Inhibition of nuclear translocation of phosphorylated STAT3 (STAT3) by 17-oxo-DHA was also demonstrated by immunoblot analysis (Fig. 3C).

3.4. The resolution of inflammation induced by UVB-irradiation was increased by 17-oxo-DHA

According to previous studies, UVB irradiation induced the generation of inflammatory cytokines in mouse skin [22]. The production of TNF-α and IL-6 (Fig. 4A), two prototypic proinflammatory cytokines, and expression of their gene transcripts (Fig. 4B) were diminished by topical application of 17-oxo-DHA. Under the same experimental conditions, there was no significant difference in the proportion of macrophages in mouse epidermis (Fig. 4C). CD36 is one of the scavenger receptors required for macrophages to detect damaged cells for adequate clearance (Fig. 4D). As shown in Fig. 4E, the expression of CD36 was significantly elevated in 17-oxo-DHA treated mouse skin.

3.5. 17-Oxo-DHA potentiated the efferocytic activity of macrophages by augmenting the expression of CD36 in BMDMs

In the resolving phase of acute inflammation, a series of steps are involved. Phagocytic removal of damaged cells by macrophages, termed 'efferocytosis', is critical to prevent the persistence of inflammation. To clarify whether 17-oxo-DHA could affect the capability of macrophages engulfing apoptotic cells, we utilized BMDMs isolated from the same strain of mice used in the *in vivo* experiments. For this purpose, JB6 murine epithelial cells were irradiated with UVB, and the resulting apoptotic JB6 cells were stained with pHrodo and co-incubated with BMDMs in the absence or presence of 5 μM 17-oxo-DHA (Fig. 5A). BMDMs with positive staining for both F4/80 (macrophage marker) and pHrodo (apoptotic cell marker) were selectively sorted by flow cytometry. As shown in Figs. 5B, 17-oxo-DHA treatment enhanced the proportion of BMDMs engulfing apoptotic epidermal cells ($F4/80^+$/$pHrodo^+$). BMDMs treated with 17-oxo-DHA displayed elevated expression of CD36 (Fig. 5C) and Nrf2 (Fig. 5D). To confirm the association between CD36 and Nrf2, immunofluorescence staining was performed with skin tissues from Nrf2 knockout (KO) and wild-type (WT) mice. F4/80 showed no significant difference between the two groups, but the expression of CD36 was decreased in Nrf2 KO mice (Fig. 5E).

3.6. The inhibition of Nrf2 restrained the effecrocytic capability of mouse BMDMs

ML385 is a chemical inhibitor of Nrf2, which is widely used to interrupt the transcription of this transcription factor. In line with this notion, the expression of Nrf2 was inhibited by pretreating BMDMs with ML385 (Fig. 6A). The proportion of BMDMs engulfing apoptotic epidermal cells was diminished by treatment with ML385 (Fig. 6B). To verify the role of Nrf2 in efferocytosis, BMDMs from Nrf2 KO mice were also employed. The 17-oxo-DHA-induced potentiation of efferocytosis was abrogated in BMDMs isolated from Nrf2 KO mice (Fig. 6C). The increase in efferocytosis activity expedites the resolution of inflammation, and this often accompanies the reduced level of inflammatory cytokines. Thus, there was significant dampening of the inhibitory effect of 17-oxo-DHA on the production of proinflammatory cytokines, TNF-α (Fig. 6D) and IL-6 (Fig. 6E), in the skin of Nrf2 KO mice.

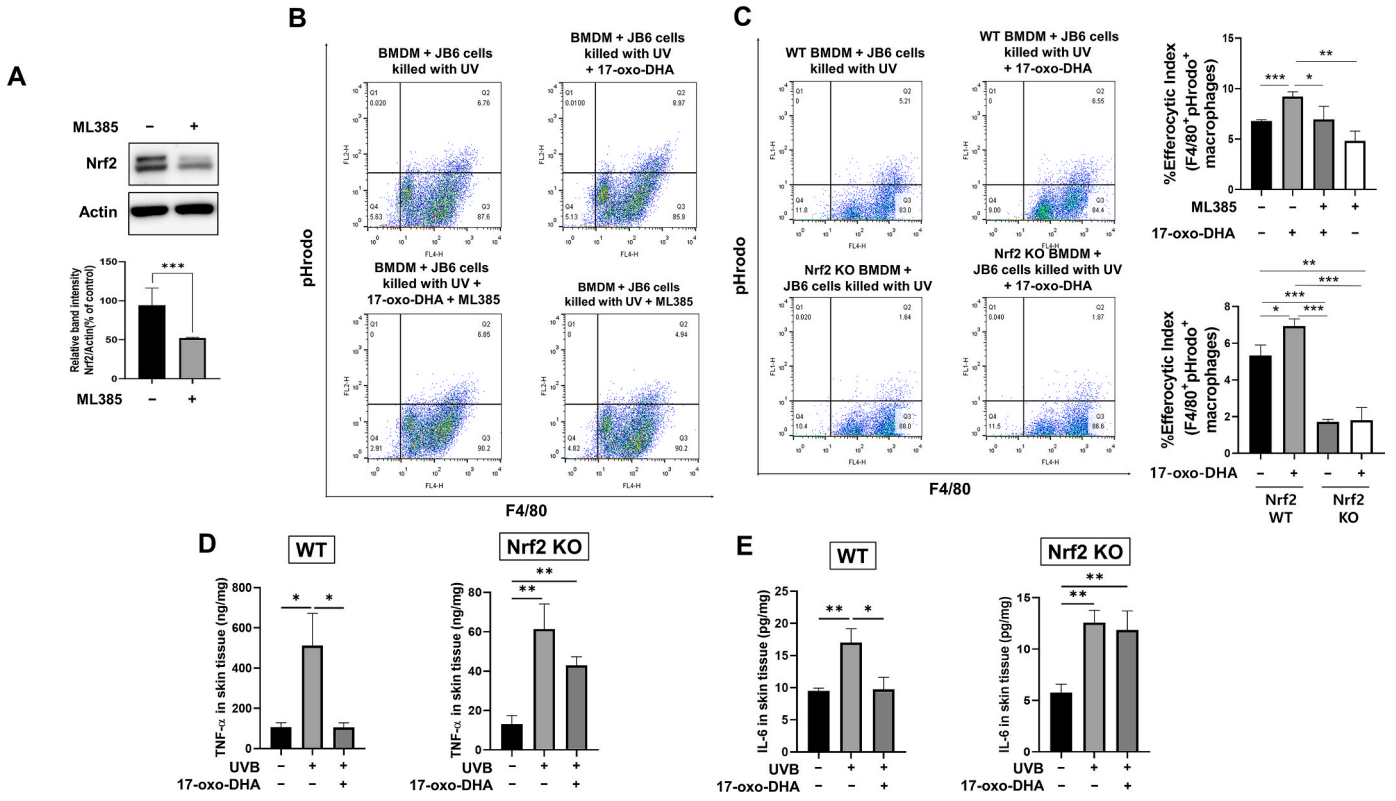

Fig. 6. Effects of pharmacologic and genetic inhibition of Nrf2 on efferocytic activity of macrophages
BMDMs were co-cultured with apoptotic epidermal JB6 cells. Before the co-incubation with dead cells, macrophages were pre-treated with a pharmacological Nrf2 inhibitor, ML385 (20 μM) for 90 min. 17-Oxo-DHA (5 μM) was added, after the wash-out with PBS for removing ML385. Twelve-hours after the incubation, BMDMs were co-cultured with pHrodo-SE-labelled apoptotic epidermal JB6 cells for 1 h. (A) The pharmacological inhibition of Nrf2 by ML385 in BMDMs was confirmed by Western blot analysis. (B) The engulfment of dead cells by macrophages was measured by flow cytometry. (C) BMDMs isolated from Nrf2 WT and KO mice were compared for their capability to engulf the apoptotic JB6 cells. (D, E) The mouse skin epidermis lysates were subjected to ELISA to measure the concentration of TNF-α (D) and IL-6 (E). Data are expressed as means ± SD (n = 3 per group). *$p < 0.05$; **$p < 0.01$; ***$p < 0.001$.

3.7. 17-Oxo-DHA protected against UVB-induced mouse skin tumor development

After confirming that the topical application of 17-oxo-DHA to the dorsal skin of mice increased the Nrf2-mediated expression of cytoprotective proteins and accelerated the resolution of inflammation, we conducted a long-term experiment to assess its chemopreventive potential against photocarcinogenesis. The results showed that UVB-induced tumor development was diminished by 17-oxo-DHA pretreatment. The body weight loss of UVB-irradiated mice was also attenuated by 17-oxo-DHA (Fig. 7A). Repeated topical application of 17-oxo-DHA before irradiation of UVB significantly reduced the number of papillomas per mouse (Fig. 7B) and the cumulative number of tumors in mouse skin (Fig. 7C). At the termination of the experiment, the total tumor burden was significantly decreased by 42.37% in the 17-oxo-DHA-treated group compared to the vehicle treated control counterparts. Notably, the number of large-sized tumors was more markedly reduced compared to that of small-sized tumors (Fig. 7D). For the growth and maintenance of tumor, blood vessels expand around the tumor, which is called angiogenesis. The topical application of 17-oxo-DHA suppressed tumor angiogenesis (Fig. 7E), and this was corroborated by the reduced amount of hemoglobin accumulated in the skin (Fig. 7F).

3.8. 17-Oxo-DHA inhibited oxidative damage and activation of STAT3 in UVB-induced mouse skin carcinogenesis

Repeated exposure to UVB radiation can lead to aggregation of the epidermal layer as verified by H&E staining (Fig. 8A). The resulting thickening of the mouse epidermis was attenuated by topically applied 17-oxo-DHA. Likewise, oxidative tissue and DNA damage were ameliorated as evidenced by the reduced expression of 4-HNE, MDA, and 8-oxo-dG (Fig. 8A). Repeated UVB irradiation resulted in over-activation of STAT3 in mouse skin through phosphorylation of Tyr705. 17-Oxo-DHA treatment significantly dampened the phosphorylation of STAT3 on Try705 and the expression of c-Myc, a major STAT3 target oncoprotein, in the skin tumor tissues (Fig. 8B).

3.9. 17-Oxo-DHA directly binds to cysteine 718 residue in STAT3 through the Michael addition reaction

The modification of proteins at critical cysteine thiols can affect the functions of many redox-sensitive proteins [28,29]. We speculated that the electrophilic α,β-unsaturated carbonyl group of 17-oxo-DHA could modify the cysteine residue of STAT3 (Fig. 9A), which might impede the phosphorylation and transcriptional activity of STAT3. As shown in Fig. 9B, STAT3 has characteristic domains and several cysteine residues.

To identify the binding site(s) of 17-oxo-DHA to STAT3 protein, LC-MS/MS analysis was performed with recombinant STAT3 protein treated with 17-oxo-DHA. First, the 17-oxo-DHA was analyzed by DIMS in the negative electrospray ionization (ESI) mode. Fragmentation MS scans were acquired by HCD of the precursor ion corresponding to 17-oxo-DHA. The MS/MS spectrum shows the information on 17-oxo-DHA (m/z 342.21) fragmentation during HCD (Supplementary Fig. 3). Secondly, peptide samples of STAT3 protein treated with 17-oxo-DHA were analyzed by LC-MS/MS. Based on the fragmentation information of 17-oxo-DHA (Supplementary Fig. 3), we were able to confirm that 17-oxo-DHA bound to the tryptic peptide derived from STAT3 protein. The

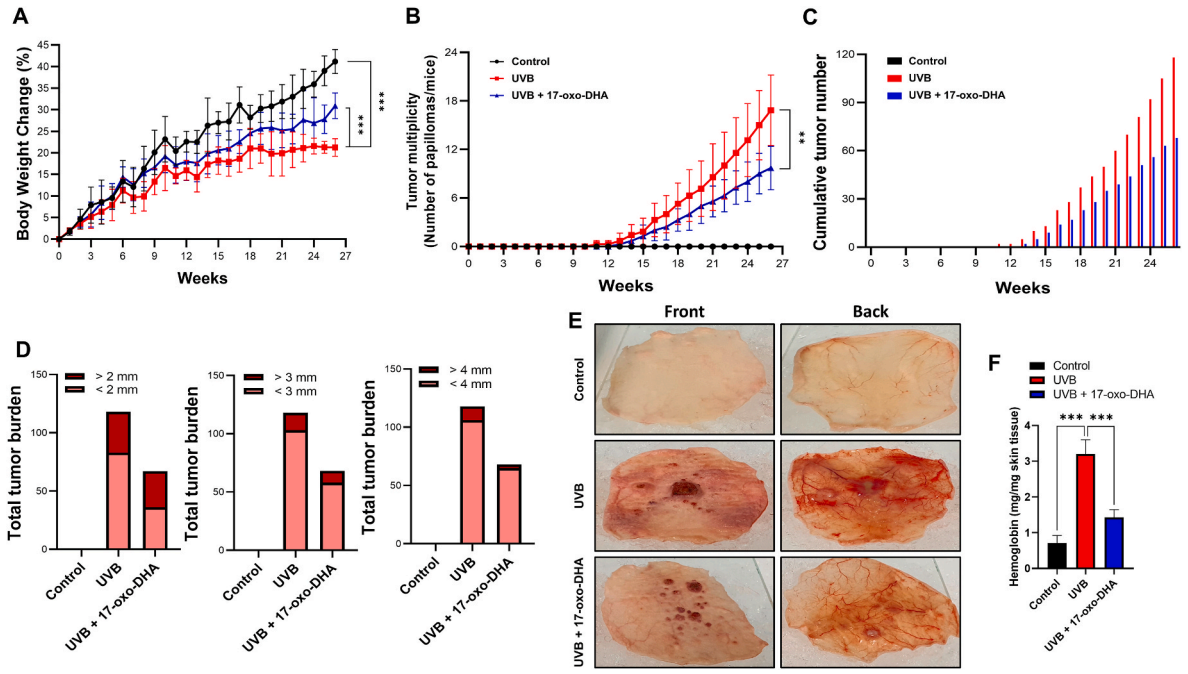

Fig. 7. Protective effects of 17-oxo-DHA against UVB-induced tumor development in hairless mouse skin
Female hairless mice were topically applied to dorsal skin with 17-oxo-DHA (20 nmol) 30 min prior to UVB irradiation (180 mJ/cm^2) three times a week until termination of the experiment on the 26th week. (A) Body weight changes during UVB-induced carcinogenesis. (B) The average number of tumors per mouse in different groups. (C) Comparison of the cumulative number of papillomas among tumor-bearing mice. (D) Tumors were counted according to the size, and the distribution of each size was calculated at the termination of the experiment is shown. (E) Photographic images represent angiogenesis, the formation of new blood vessels, around the skin tumors. (F) Amount of hemoglobin in UVB-induced mouse skin tissues was measured by Drabkin's reagent as described in Materials and Methods. Data are expressed as means ± SD (n = 7 per group). $^{**}p < 0.01$; $^{***}p < 0.001$.

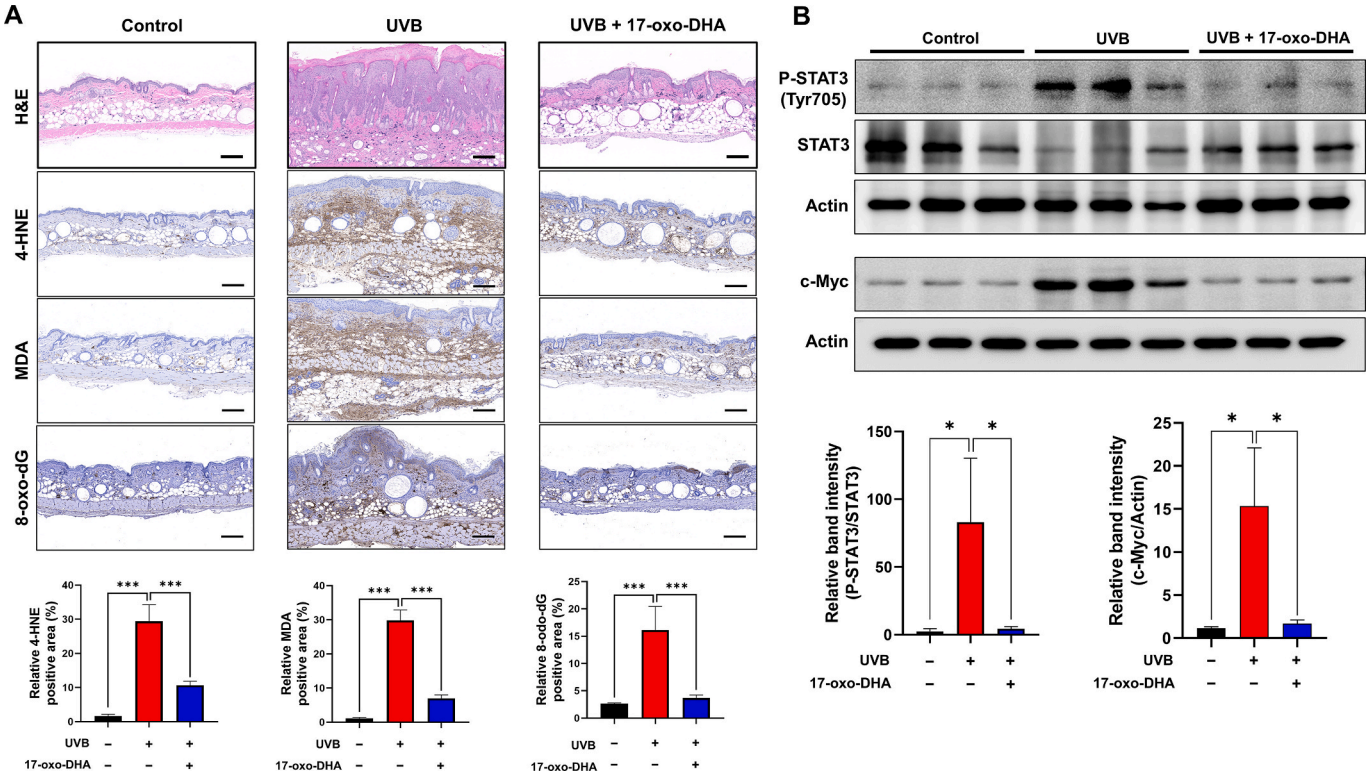

Fig. 8. Attenuation of long-term UVB-induced oxidative skin damage in 17-oxo-DHA treated mice.
Tissues collected mice from the long-term tumor experiments were saved and subjected to histological, immunohistochemical and immune blot analyses. (A) Skin thickness and hyperplasia were confirmed by H&E staining. Immunohistochemical analysis of 4-HNE, MDA, and 8-oxo-dG in mouse epidermis. Manification, 100 X; Scale bar, 200 μm. (B) The phosphorylation of STAT3 and expression of its target protein, c-Myc were measured by immunoblot analysis. Data are expressed as means ± SD (n = 3 per group). $^{*}p < 0.05$; $^{***}p < 0.001$.

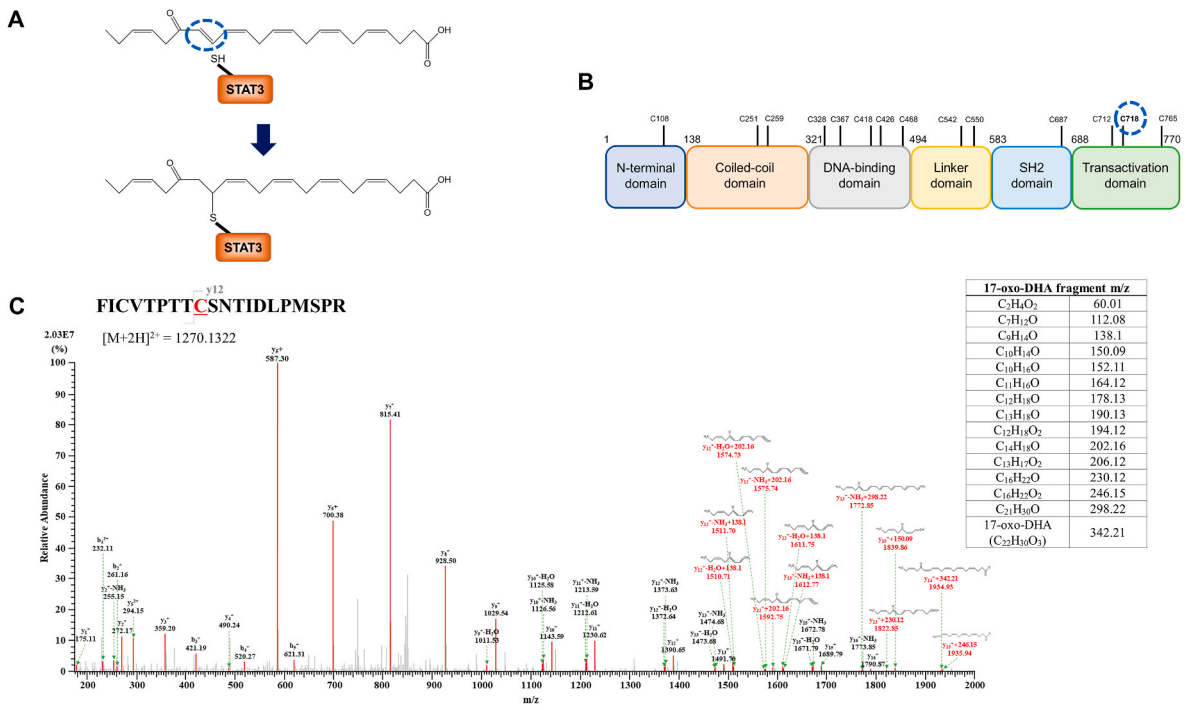

Fig. 9. Mass spectrometric analysis of covalent modification of STAT3 by 17-oxo-DHA. (A) The expected interaction between a thiol group of STAT3 and 17-oxo-DHA. (B) Schematic domain structure of STAT3, which contains six different unique functions. (C) Mass spectral identification of STAT3 peptide (FICVTPTTCSNTIDLPMSPR) covalently modified by 17-oxo-DHA. Annotated LC-MS/MS spectrum illustrating the binding of 17-oxo-DHA to STAT3 protein at Cys718 residues. The precursor ion for a peptide with 17-oxo-DHA binding is $[M+2H]^{2+}$ (*m/z* 1270.1322). The list of elucidated 17-oxo-DHA fragmentation is inserted into the spectrum as a table. The molecular symbol labelled with y ion on the spectrum represents the fragment ion of 17-oxo-DHA bound to Cys718.

molecular ion matching to $[M+2H]^{2+}$ (*m/z* 1270.1322) of 710-FICVTPTTCSNTIDLPMSPR-729 was acquired, indicative of STAT3 modified by 17-oxo-DHA at the cysteine 718 (Cys718) residue (Fig. 9C).

4. Discussion

The chemopreventive and anti-carcinogenic activities of DHA have been reported [30,31]. DHA has a potential as an adjuvant and therapeutic agent in the management of skin disorders such as dermatitis and photocarcinogenesis [22,31,32]. Because of its hydrophobic nature, DHA can readily penetrate the skin, and can be absorbed into skin cells [33]. However, it remains poorly understood whether the anti-inflammatory and chemopreventive effects of DHA are mediated directly by this fatty acid or via metabolism. A series of electrophilic metabolites of DHA and other ω-3 polyunsaturated fatty acids have been reported to exert pleiotropic anti-inflammatory effects [23–25] and also anti-carcinogenic activity [26].

17-Oxo-DHA is an endogenous electrophilic derivative of DHA which is produced in activated macrophages via sequential enzymatic reactions catalyzed by COX-2 and dehydrogenase [23]. When DHA was topically applied onto mouse skin, 17-oxo-DHA as well as an intermediary metabolite 17-hydroxy-DHA was generated (S.-H. Kim & Y.-J. Surh, unpublished observation). Because of the electrophilic α,β-unsaturated carbonyl moiety, 17-oxo-DHA is anticipated to covalently bind to a sensor cysteine residue of Keap1, thereby activating Nrf2 [34]. In our previous study, 17-oxo-DHA was found to inhibit the Keap1-dependent ubiquitination of Nrf2 through modification of the Cys151 or Cys273 residues of Keap1 [34]. As a result, nuclear translocation and transcriptional activity of Nrf2 were enhanced, followed by upregulation of HO-1 expression in murine epidermal cells. Notably, direct topical application of 17-oxo-DHA exerted anti-inflammatory effects in UVB-irradiated mouse skin at a much smaller dose than that of the parent compound, DHA [34].

Failure to resolve acute inflammation (unresolving inflammation) leads to chronic disorders, such as arthritis, asthma, psoriasis, and carcinogenesis [35–38]. The resolution of inflammation relates to the capacity of macrophages to use the substances derived from the phagolysosomal hydrolysis of apoptotic cells as the fuel of efferocytosis [39,40]. Through this efferocytic ability, activated macrophages accelerate the resolution of inflammation, prevent cell destruction and release of toxic substances, and increase the production of anti-inflammatory cytokines, including IL-10 and TGF-β [41]. 17-Oxo-DHA suppresses the release of the proinflammatory cytokine, IL-1β through inhibition of NLRP3 inflammasomes [25] and exerts antioxidant effects in immune and structural cells [24]. Though *in vitro* studies using 17-oxo-DHA have been conducted [24,25,34], its anti-inflammatory effect *in vivo* has not been reported yet.

Proinflammatory cytokines, chemokines and other mediators are involved in the inflammatory tumor microenvironment [42], and STAT3 is essential for regulating their expression [27,43,44]. The extrinsic inflammatory factors such as chemical carcinogens, pathogens and UVB can activate STAT3 via different pathways [45–48]. Thus, inhibition of aberrant STAT3 activation is considered a practical therapeutic approach for achieving the prevention of inflammation-associated carcinogenesis. Repression of STAT3 overactivation can be achieved not only by inhibiting upstream signaling pathways such as Janus kinase, epidermal growth factor receptor, and IL-6R [49], but also through direct covalent modification of specific cysteine thiol residues.

STAT3 contains 14 highly conserved cysteine residues of which nine are reported to be redox-sensitive and critical in controlling its transcriptional activity [50]. Previous studies in our laboratory demonstrated that the cysteine 259 residue of STAT3 was directly modified by the natural polyphenolic compound, curcumin harbouring an α,β-unsaturated carbonyl moiety [51] or some electrophilic prostaglandin metabolites of arachidonic acid, which hampered the phosphorylation and consequently the activation of STAT3 [52,53]. Unlike these compounds, however, 17-oxo-DHA was found to preferentially bind to the Cys718 residue of STAT3. To the best of our knowledge, this

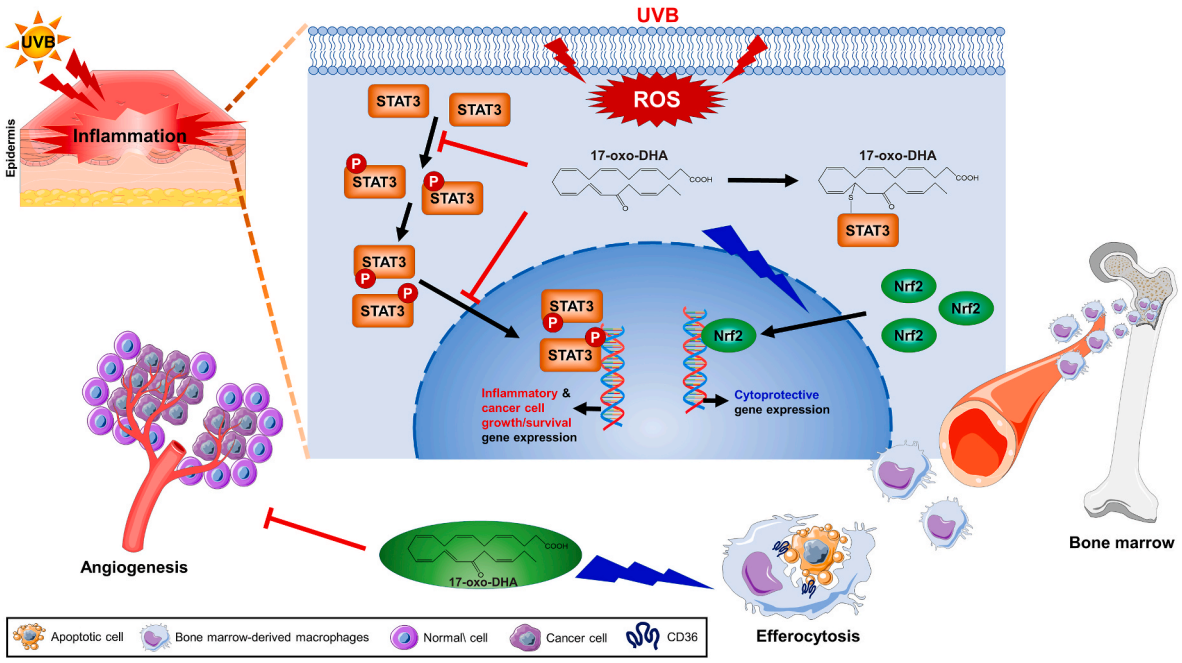

Fig. 10. A schematic representation of the molecular mechanism underlying protective effects of 17-oxo-DHA against UVB-induced dermatitis and skin carcinogenesis.

is the first demonstration of the posttranslational modification of STAT3 at this particular amino acid.

The STAT3 protein consists of 6 domains with different functions and roles [54]. Cys718 is present in the highly conserved but intrinsically disordered C-terminal transactivation domain (TAD) that is important for dimerization, nuclear translocation, and full transcriptional activity of STAT3 [55]. STAT3 activation is dependent on the Tyr705 residue, an essential site for phosphorylation and dimerization of STAT3 [56]. We speculate that covalent modification of Cys718 by 17-oxo-DHA may induce a change in the structure of STAT3, which hinders its accessibility to the upstream kinase, Janus kinase (JAK), thereby protecting the Tyr705 residue from phosphorylation. In support of this speculation, cysteine thiol modification in the TAD domain inhibited phosphorylation and nuclear localization of STAT3 without influencing the expression/activity of JAK1 and 2 [57]. Of note, Cys718 has been suggested to be involved in STAT3 dimerization and also in interaction with other proteins such peroxiredoxin-2 [58]. Further studies will be necessary to precisely elucidate the mechanisms underlying how Cys718 modification by 17-oxo-DHA can affect the STAT3 signaling.

Macrophages detect and engulf apoptotic cells through sequential mechanisms including the recognition of phosphatidylserine via scavenger receptors [59]. The contribution of CD36, one of the principal scavenger receptors present in macrophages, to the resolution of inflammation has been continuously reported [60,61]. In the present study, the role of Nrf2 in CD36-mediated effecrocytosis was assessed by use of an Nrf2 inhibitor and Nrf2 deficient mice. BMDMs subjected to chemical inhibition and genetic deficiency of Nrf2 exacerbated efferocytic activity of macrophages, which was ascribed to repression of CD36 expression. It is noticeable that HO-1, which is upregulated via the Nrf2 signal pathway, has been reported to potentiate the efferocytic activity of macrophages by elevating the expression of scavenger receptors including CD36 and dectin-1 [62,63].

In conclusion, the topical application of 17-oxo-DHA protects against UVB-induced dermatitis and carcinogenesis via suppression of the STAT3 pathway, and activation of the Nrf2/ARE signaling (Fig. 10). Nrf2 activation promoted the resolution of skin inflammation through potentiation of efferocytic activity of macrophages phagocytosing apoptotic epidermal cells which was attributed to upregulated CD36 expression responsible for recognition and elimination of dead/dying cells. Therefore, 17-oxo-DHA can be suggested as a candidate for the chemoprotection/chemoprevention of UVB-induced dermitis and photocarcinogenesis.

Declaration of competing interest

The authors declare that they have no conflict of interest in this paper.

Data availability

Data will be made available on request.

Acknowledgements

This study was supported by INTERNATIONAL COOPERATION Program (2021K2A9A1A0609657411 to Y.-J.Surh) from the National Research Foundation, Republic of Korea, the Scientific and Technological Research Council of Turkey (TUBITAK) (221N049 to N. K. Özer), Basic Science Research Grant (2021R1I1A1A0104654012 to S.-J. Kim) from the National Research Foundation, Republic of Korea, and Bio & Medical Technology Development Program (NRF-2019M3E5D3073567 to K. P. Kim) from the National Research Foundation, Republic of Korea.

Appendix A. Supplementary data

Supplementary data to this article can be found online at https://doi.org/10.1016/j.redox.2023.102666.

References

[1] C. Blanpain, E. Fuchs, Epidermal homeostasis: a balancing act of stem cells in the skin, Nat. Rev. Mol. Cell Biol. 10 (3) (2009) 207–217.
[2] E. Fuchs, Finding one's niche in the skin, Cell Stem Cell 4 (6) (2009) 499–502.
[3] K. Honda, D.R. Littman, The microbiota in adaptive immune homeostasis and disease, Nature 535 (7610) (2016) 75–84.
[4] M. Pasparakis, Regulation of tissue homeostasis by NF-κB signalling: implications for inflammatory diseases, Nat. Rev. Immunol. 9 (11) (2009) 778–788.

[5] V. Horsley, Skin in the game: stem cells in repair, cancer, and homeostasis, Cell 181 (3) (2020) 492–494.
[6] G.T. Bowden, Prevention of non-melanoma skin cancer by targeting ultraviolet-B-light signalling, Nat. Rev. Cancer 4 (1) (2004) 23–35.
[7] D.S. Rigel, Cutaneous ultraviolet exposure and its relationship to the development of skin cancer, J. Am. Acad. Dermatol. 58 (5 Suppl 2) (2008) S129–S132.
[8] M. Pasparakis, I. Haase, F.O. Nestle, Mechanisms regulating skin immunity and inflammation, Nat. Rev. Immunol. 14 (5) (2014) 289–301.
[9] A. Mantovani, M.A. Cassatella, C. Costantini, S. Jaillon, Neutrophils in the activation and regulation of innate and adaptive immunity, Nat. Rev. Immunol. 11 (8) (2011) 519–531.
[10] G. Majno, I. Joris, Cells, Tissues, and Disease: Principles of General Pathology, second ed., Oxford University Press, New York, 2004.
[11] L.M. Coussens, Z. Werb, Inflammation and cancer, Nature 420 (6917) (2002) 860–867.
[12] M.R. Elliott, K.M. Koster, P.S. Murphy, Efferocytosis signaling in the regulation of macrophage inflammatory responses, J. Immunol. 198 (4) (2017) 1387–1394.
[13] E. Boada-Romero, J. Martinez, B.L. Heckmann, D.R. Green, The clearance of dead cells by efferocytosis, Nat. Rev. Mol. Cell Biol. 21 (7) (2020) 398–414.
[14] A.C. Doran, A. Yurdagul Jr., I. Tabas, Efferocytosis in health and disease, Nat. Rev. Immunol. 20 (4) (2020) 254–267.
[15] T. Bowman, M.A. Broome, D. Sinibaldi, W. Wharton, W.J. Pledger, J.M. Sedivy, R. Irby, T. Yeatman, S.A. Courtneidge, R. Jove, Stat3-mediated Myc expression is required for Src transformation and PDGF-induced mitogenesis, Proc. Natl. Acad. Sci. U.S.A. 98 (13) (2001) 7319–7324.
[16] H. Yu, H. Lee, A. Herrmann, R. Buettner, R. Jove, Revisiting STAT3 signalling in cancer: new and unexpected biological functions, Nat. Rev. Cancer 14 (11) (2014) 736–746.
[17] J.D. Hayes, A.T. Dinkova-Kostova, The Nrf2 regulatory network provides an interface between redox and intermediary metabolism, Trends Biochem. Sci. 39 (4) (2014) 199–218.
[18] F. He, X. Ru, T. Wen, NRF2, a transcription factor for stress response and beyond, Int. J. Mol. Sci. 21 (13) (2020) 4777.
[19] C.N. Serhan, Pro-resolving lipid mediators are leads for resolution physiology, Nature 510 (7503) (2014) 92–101.
[20] M.C. Basil, B.D. Levy, Specialized pro-resolving mediators: endogenous regulators of infection and inflammation, Nat. Rev. Immunol. 16 (1) (2016) 51–67.
[21] I. Tabas, C.K. Glass, Anti-inflammatory therapy in chronic disease: challenges and opportunities, Science 339 (6116) (2013) 166–172.
[22] H.W. Yum, J. Park, H.J. Park, J.W. Shin, Y.Y. Cho, S.J. Kim, J.X. Kang, Y.J. Surh, Endogenous omega-3 fatty acid production by *fat-1* transgene and topically applied docosahexaenoic acid protect against UVB-induced mouse skin carcinogenesis, Sci. Rep. 7 (1) (2017), 11658.
[23] A.L. Groeger, C. Cipollina, M.P. Cole, S.R. Woodcock, G. Bonacci, T.K. Rudolph, V. Rudolph, B.A. Freeman, F.J. Schopfer, Cyclooxygenase-2 generates anti-inflammatory mediators from omega-3 fatty acids, Nat. Chem. Biol. 6 (6) (2010) 433–441.
[24] C. Cipollina, S. Di Vincenzo, S. Gerbino, L. Siena, M. Gjomarkaj, E. Pace, Dual anti-oxidant and anti-inflammatory actions of the electrophilic cyclooxygenase-2-derived 17-oxo-DHA in lipopolysaccharide- and cigarette smoke-induced inflammation, Biochim. Biophys. Acta 1840 (7) (2014) 2299–2309.
[25] C. Cipollina, S. Di Vincenzo, L. Siena, C. Di Sano, M. Gjomarkaj, E. Pace, 17-oxo-DHA displays additive anti-inflammatory effects with fluticasone propionate and inhibits the NLRP3 inflammasome, Sci. Rep. 6 (2016), 37625.
[26] L. Siena, C. Cipollina, S. Di Vincenzo, M. Ferraro, A. Bruno, M. Gjomarkaj, E. Pace, Electrophilic derivatives of omega-3 fatty acids counteract lung cancer cell growth, Cancer Chemother. Pharmacol. 81 (4) (2018) 705–716.
[27] H. Yu, D. Pardoll, R. Jove, STATs in cancer inflammation and immunity: a leading role for STAT3, Nat. Rev. Cancer 9 (11) (2009) 798–809.
[28] C.L. Oeste, D. Perez-Sala, Modification of cysteine residues by cyclopentenone prostaglandins: interplay with redox regulation of protein function, Mass Spectrom. Rev. 33 (2) (2014) 110–125.
[29] C.E. Paulsen, K.S. Carroll, Cysteine-mediated redox signaling: chemistry, biology, and tools for discovery, Chem. Rev. 113 (7) (2013) 4633–4679.
[30] L.A. Horrocks, Y.K. Yeo, Health benefits of docosahexaenoic acid (DHA), Pharmacol. Res. 40 (3) (1999) 211–225.
[31] H.W. Yum, H.K. Na, Y.J. Surh, Anti-inflammatory effects of docosahexaenoic acid: implications for its cancer chemopreventive potential, Semin. Cancer Biol. 40–41 (2016) 141–159.
[32] A.P. Simopoulos, Omega-3 fatty acids in inflammation and autoimmune diseases, J. Am. Coll. Nutr. 21 (6) (2002) 495–505.
[33] P.C. Calder, Docosahexaenoic acid, Ann. Nutr. Metab. 69 (Suppl 1) (2016) 7–21.
[34] M.U. Jamil, J. Kim, H.W. Yum, S.H. Kim, S.J. Kim, D.H. Kim, N.C. Cho, H.K. Na, Y. J. Surh, 17-Oxo-docosahexaenoic acid induces Nrf2-mediated expression of heme oxygenase-1 in mouse skin in vivo and in cultured murine epidermal cells, Arch. Biochem. Biophys. 679 (2020), 108156.
[35] C.D. Buckley, D.W. Gilroy, C.N. Serhan, B. Stockinger, P.P. Tak, The resolution of inflammation, Nat. Rev. Immunol. 13 (1) (2013) 59–66.
[36] G. Schett, D. Elewaut, I.B. McInnes, J.M. Dayer, M.F. Neurath, How cytokine networks fuel inflammation: toward a cytokine-based disease taxonomy, Nat. Med. 19 (7) (2013) 822–824.
[37] I.B. McInnes, G. Schett, Pathogenetic insights from the treatment of rheumatoid arthritis, Lancet 389 (10086) (2017) 2328–2337.
[38] C. Nathan, A. Ding, Nonresolving inflammation, Cell 140 (6) (2010) 871–882.
[39] A. Hochreiter-Hufford, K.S. Ravichandran, Clearing the dead: apoptotic cell sensing, recognition, engulfment, and digestion, Cold Spring Harbor Perspect. Biol. 5 (1) (2013) a008748.
[40] D.R. Green, T.H. Oguin, J. Martinez, The clearance of dying cells: table for two, Cell Death Differ. 23 (6) (2016) 915–926.
[41] D. Korns, S.C. Frasch, R. Fernandez-Boyanapalli, P.M. Henson, D.L. Bratton, Modulation of macrophage efferocytosis in inflammation, Front. Immunol. 2 (2011) 57.
[42] H. Yu, M. Kortylewski, D. Pardoll, Crosstalk between cancer and immune cells: role of STAT3 in the tumour microenvironment, Nat. Rev. Immunol. 7 (1) (2007) 41–51.
[43] P.C. Heinrich, I. Behrmann, S. Haan, H.M. Hermanns, G. Muller-Newen, F. Schaper, Principles of interleukin (IL)-6-type cytokine signalling and its regulation, Biochem. J. 374 (Pt 1) (2003) 1–20.
[44] Z. Zhong, Z. Wen, J.E. Darnell Jr., Stat3: a STAT family member activated by tyrosine phosphorylation in response to epidermal growth factor and interleukin-6, Science 264 (5155) (1994) 95–98.
[45] M. Gu, R.P. Singh, S. Dhanalakshmi, C. Agarwal, R. Agarwal, Silibinin inhibits inflammatory and angiogenic attributes in photocarcinogenesis in SKH-1 hairless mice, Cancer Res. 67 (7) (2007) 3483–3491.
[46] C.N. Landen Jr., Y.G. Lin, G.N. Armaiz Pena, P.D. Das, J.M. Arevalo, A.A. Kamat, L. Y. Han, N.B. Jennings, W.A. Spannuth, P.H. Thaker, S.K. Lutgendorf, C.A. Savary, A.M. Sanguino, G. Lopez-Berestein, S.W. Cole, A.K. Sood, Neuroendocrine modulation of signal transducer and activator of transcription-3 in ovarian cancer, Cancer Res. 67 (21) (2007) 10389–10396.
[47] J. Arredondo, A.I. Chernyavsky, D.L. Jolkovsky, K.E. Pinkerton, S.A. Grando, Receptor-mediated tobacco toxicity: cooperation of the Ras/Raf-1/MEK1/ERK and JAK-2/STAT-3 pathways downstream of alpha7 nicotinic receptor in oral keratinocytes, Faseb. J. 20 (12) (2006) 2093–2101.
[48] D.M. Bronte-Tinkew, M. Terebiznik, A. Franco, M. Ang, D. Ahn, H. Mimuro, C. Sasakawa, M.J. Ropeleski, R.M. Peek Jr., N.L. Jones, Helicobacter pylori cytotoxin-associated gene A activates the signal transducer and activator of transcription 3 pathway in vitro and in vivo, Cancer Res. 69 (2) (2009) 632–639.
[49] D.E. Johnson, R.A. O'Keefe, J.R. Grandis, Targeting the IL-6/JAK/STAT3 signalling axis in cancer, Nat. Rev. Clin. Oncol. 15 (4) (2018) 234–248.
[50] F.A. Zouein, R. Altara, Q. Chen, E.J. Lesnefsky, M. Kurdi, G.W. Booz, Pivotal importance of STAT3 in protecting the heart from acute and chronic stress: new advancement and unresolved issues, Front. Cardiovasc. Med. 2 (2015) 36.
[51] Y.I. Hahn, S.J. Kim, B.Y. Choi, K.C. Cho, R. Bandu, K.P. Kim, D.H. Kim, W. Kim, J. S. Park, B.W. Han, J. Lee, H.K. Na, Y.N. Cha, Y.J. Surh, Curcumin interacts directly with the Cysteine 259 residue of STAT3 and induces apoptosis in H-Ras transformed human mammary epithelial cells, Sci. Rep. 8 (1) (2018) 6409.
[52] S.J. Kim, N.C. Cho, B. Han, K. Kim, Y.I. Hahn, K.P. Kim, Y.G. Suh, B.Y. Choi, H. K. Na, Y.J. Surh, 15-Deoxy-$\Delta^{12,14}$-prostaglandin J_2 binds and inactivates STAT3 via covalent modification of cysteine 259 in H-Ras-transformed human breast epithelial cells, FEBS Lett. 595 (5) (2021) 604–622.
[53] E.J. Lee, S.J. Kim, Y.I. Hahn, H.J. Yoon, B. Han, K. Kim, S. Lee, K.P. Kim, Y.G. Suh, H.K. Na, Y.J. Surh, 15-Keto prostaglandin E_2 suppresses STAT3 signaling and inhibits breast cancer cell growth and progression, Redox Biol. 23 (2019), 101175.
[54] S. Zou, Q. Tong, B. Liu, W. Huang, Y. Tian, X. Fu, Targeting STAT3 in cancer immunotherapy, Mol. Cancer 19 (1) (2020) 145.
[55] J. Sgrignani, M. Garofalo, M. Matkovic, J. Merulla, C.V. Catapano, A. Cavalli, Structural biology of STAT3 and its implications for anticancer therapies development, Int. J. Mol. Sci. 19 (6) (2018).
[56] D.E. Levy, C.K. Lee, What does Stat3 do? J. Clin. Invest. 109 (9) (2002) 1143–1148.
[57] X. Yu, L. He, P. Cao, Q. Yu, Eriocalyxin B inhibits STAT3 signaling bycovalently targeting STAT3 and blocking phosphorylation and activation of STAT3, PLoS One 10 (5) (2015), e0128406.
[58] M.C. Sobotta, W. Liou, S. Stocker, D. Talwar, M. Oehler, T. Ruppert, A.N. Scharf, T. P. Dick, Peroxiredoxin-2 and STAT3 form a redox relay for H_2O_2 signaling, Nat. Chem. Biol. 11 (1) (2015) 64–70.
[59] G. Lemke, How macrophages deal with death, Nat. Rev. Immunol. 19 (9) (2019) 539–549.
[60] M.S. Woo, J. Yang, C. Beltran, S. Cho, Cell surface CD36 protein in monocyte/macrophage contributes to phagocytosis during the resolution phase of ischemic stroke in mice, J. Biol. Chem. 291 (45) (2016) 23654–23661.
[61] Y.M. Park, CD36, a scavenger receptor implicated in atherosclerosis, Exp. Mol. Med. 46 (2014) e99.
[62] S.H. Kim, X. Zhong, W. Kim, K. Kim, Y.G. Suh, C. Kim, Y. Joe, H.T. Chung, Y. N. Cha, Y.J. Surh, Taurine chloramine potentiates phagocytic activity of peritoneal macrophages through up-regulation of dectin-1 mediated by heme oxygenase-1-derived carbon monoxide, Faseb. J. 32 (4) (2018) 2246–2257.
[63] T. Ishii, K. Itoh, E. Ruiz, D.S. Leake, H. Unoki, M. Yamamoto, G.E. Mann, Role of Nrf2 in the regulation of CD36 and stress protein expression in murine macrophages: activation by oxidatively modified LDL and 4-hydroxynonenal, Circ. Res. 94 (5) (2004) 609–616.